JOURNAL OF PROPULSION AND POWER
Vol. 12, No. 1, January–February 1996

Model Developments for the Brush Seal Numerical Simulation

V. V. Kudriavtsev* and M. J. Braun†
University of Akron, Akron, Ohio 44325

A general review of the experimental, numerical/analytical, and industrial state of the art in the development of brush seals is presented. The authors formulate a numerical model as it relates to the physics of the flow, as understood from the numerous experiments done in the hydraulic tunnel at the University of Akron. Based further on their own experimental and numerical work, the authors propose a new approach to the numerical flow simulation of full brushes. This approach involves the segmentation of the brush in repetitive core segments, bound by an inlet and an exit segment. A numerical experiment is performed to prove the validity of the concept.

Nomenclature

d	=	pin diameter, m
h	=	channel height, $h = L_y = L_0$, m
N_{rows}	=	number of rows in a cylinder array
N^{seg}	=	number of the brush segments
P	=	nondimensional pressure, $P_0 = \rho U_0^2$, p/P_0
$PTDR_L$	=	longitudinal pitch-to-diameter ratio, S_L/d
$PTDR_T$	=	transversal pitch-to-diameter ratio, S_T/d
p	=	pressure, Pa
Re	=	Reynolds number based on channel width/height, $U_0 h/\nu$
Re_d	=	Reynolds number based on pin diameter, $U_0 d\rho/\mu$
S_L	=	longitudinal pitch, m
S_T	=	transversal pitch, m
T	=	time, tT_0, s
T_0	=	time scale, L_0/U_0, s
t	=	nondimensional time
U	=	velocity in X direction, uU_0, m/s
U_0	=	freestream velocity, m/s
u, v	=	nondimensional fluid velocities
V	=	velocity in Y direction, vU_0, m/s
x	=	dimensionless coordinate, X/L_0
y	=	dimensionless coordinate, Y/L_0
Δx	=	minimum grid size in x direction
Δy	=	minimum grid size in y direction
$\Delta\tau$	=	nondimensional time step
σ	=	pseudotime step, the pressure equation

I. Introduction

THE development of the brush seal is considered to be most promising among the advanced type seals that are presently in use in high-speed turbomachinery. The brush is usually mounted on the stationary portions of the engine and has direct contact with the rotating elements, thus limiting the "unwanted" leakage flows between stages or various engine cavities. This type of sealing technology (in comparison with conventional seals) is providing high-pressure drops due mainly to the high packing density (around 100 bristles/1 mm^2) and brush compliance with the rotor motions. In the design of modern turbomachinery, leakage flows between the stages must be minimal, thus contributing to the higher efficiency of the engine. Use of the brush seal instead of the labyrinth seal reduces the leakage flow by one degree of magnitude.[1,2] Brush seals were also found to enhance dynamic performance, cost less, and be lighter than labyrinth seals. Even though, industrially, brush seals have been successfully developed through extensive experimentation,[1,2] there is no comprehensive numerical methodology for the design or prediction of their performance.[3–5] The existing analytical/numerical approaches are based on bulk flow models[6,7] and do not allow the investigation of the effects of brush morphology (bristle arrangement), or brushes arrangement (number of brushes, spacing between them), on the pressure drops and flow leakage. An increase in the brush seal efficiency is clearly a complex problem that is closely related to the brush geometry and morphology, and most likely can be solved only by means of a numerically distributed model.

II. Brief Review of the State of the Art

Experiments done by Cross Mfg.[8] (CM) showed that the leakages in brushes are approximately 5–10% of a finned labyrinth configuration. The brushes manufactured by CM have been eventually incorporated in the Rolls Royce design of the IAE V2500-A1. As reported by Withers,[2] it was observed that the seals quickly ran into a stabilized steady configuration, and thus could, potentially, run indefinitely with minimum maintenance.

Allison Engine Company also reported successful incorporation of brush seals in some of their engines. According to Holle and Krishnan,[9] the T800 engine was tested with a brush seal located at the turbine discharge, whereas the T406 Plus engine contained 13 brush seals between the compressor interstages. Experiments performed at Teledyne CAE[10] showed that the leakages may be reduced by a factor of 4 to 7, and that the leakage (vs pressure drop) performance often follows a hysteresis curve. It was also reported that the brush seals were able to survive shaft excursions of over 0.0025 in. without any significant loss in performance.[10,11] Recent reports from Wright–Patterson AFB[11] describe efforts for the incorporation of brush seals in all demonstrator engines and the replacement of the labyrinth seals with brush seals at all compressor interstage locations. The experimental Advanced Brush Seal Development Program at EG&G Fluid Components generated a comprehensive design methodology[12] for application to high-performance brush seals. Work done at Texas A&M[13] reported that 1) the last stage of the seals' group develops a higher pressure drop than the previous stages and 2) generally, seals improve rotordynamic characteristics. Caroll and Easter[14] proposed a brush seal that would prevent a recirculating flow of hot combustion gases from reaching a bellows seal located in the wall of a combustion chamber. Braun et al.[15] studied nonintrusively the fundamental flow patterns and reconstructed graphically the fluid velocities inside a cascade of brushes. The flowfield was visualized by means of the full

Received July 28, 1994; revision received April 24, 1995; accepted for publication May 3, 1995.

*Department of Mechanical Engineering; currently Research Engineer, B&C Engineering Associates, Akron, OH. Member AIAA.
†Professor, Department of Mechanical Engineering.

flow field tracking (FFFT) method,[15] and revealed regions that are characteristically river jetting, vortical, crossflow, and exist upstream, downstream, or within the seal. It has been found that high brush resistance to flow can result in sudden catastrophic failure of the seal, whereas at lower flow resistance the failure is gradual.

Presently, there is a strong ongoing theoretical effort to simulate the hydraulic performance of the brush. Hendricks and Braun[7] have developed a bulk flow model based on the porosity concept. The analysis predicts the pressure and leakage performance as a function of bristles' configuration, porosity, deformation, interface loading, and type of interference with the rotating shaft. Trendwise, for the interference fit, these results compare favorably with experimental results reported by Flower,[8] even though the abrupt changes predicted by the bulk-flow model do not appear in Flower's reported data. Another leakage flow model is reported by Chupp et al.[6] While the basic premise of the model is similar to that of Ref. 7, the only parameter considered is the effective brush thickness. However, bulk models[6,7] and empirical formulas for the pressure drops in tube arrays[17] cannot fully account for the brush geometry effects and cannot predict local brush compliance or the associated flow phenomena.

Conclusions of a recent NASA seal workshop[5] indicate that while the brush seals work well, there is a need to improve its performance characteristics. Such a goal can be achieved by using cascades of brushes, nonhomogeneous brush morphology, nonconventional brush structure design, and in general, a process of optimization of brush design parameters. The distributed velocity fields (u, v) and the associated pressure distributions are of vital importance for the prediction of the average pressure drop or the possible sudden failure of the brush seal under unexpected local pressure fluctuations.

III. Problem Definition

The design goals of the model aim at determining the pressure drop for a configuration specified by the designer. That includes the density of the brush packaging, length, number of rows, bristles sizes (homogeneous or nonhomogeneous), and distances between the rows, or brushes, respectively (single, double, or cascade brush). The systemic goals are to 1) develop a physically relevant package of assumptions for the simulation of the brush seal and to implement a robust numerical method (using primitive variables u, v, and p) for the calculation of the forced convective flow through dense brush-like cylinder arrays and 2) analyze numerically different aspects of the flow dynamics in the generic brush prototypes.

For analysis and classification purposes we identified four different models of generic brush geometries.[18] The simplest model (level 1) assumes flow analysis in the vicinity of a nonmoving single bristle.[19] The second level (level 2) model introduces the analysis of a limited cluster that consists of several nonmoving bristles,[18,19] that do influence jointly the flowfield through disturbances generated by the wake vortices. Level 3 introduces the analysis for a multicluster,[20] and finally, level 4 assembles large numbers of clusters with small pitch-to-diameter ratio *PTDR* that actually simulate the real brush.[21]

One can see an idealized schematic of a linear brush seal in Fig. 1. In real conditions the flow upstream of the seal exhibits both circumferential and axial components. Reynolds numbers typical for the circumferential component are usually in the range 10^4–10^6, while for the transversal component (leakage flow) they do not exceed low laminar values. Recently published data[6,10,11] allowed us to determine the typical ranges of the parameters that characterize the brush seals tested by the industry. The level of the leakage flow u_{leak} and maximum velocity in the bristles pitch u_{max} were estimated as 3.17 and 76.55 m/s, respectively. In Fig. 2 one can find an approximate range of Reynolds numbers typical for a brush seal functioning in air (results were obtained based on the

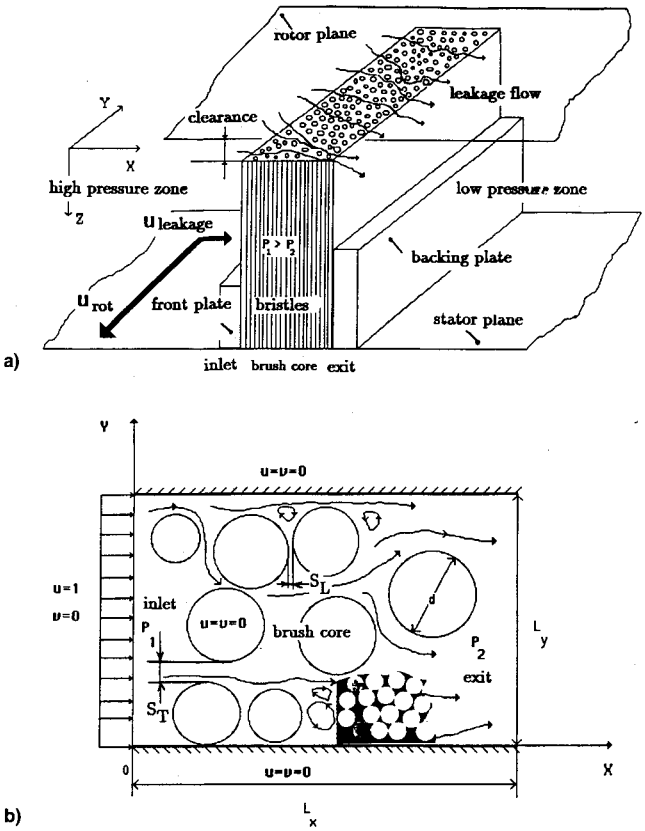

Fig. 1 Idealized schematic of the brush seal and flow path: a) generic seal and b) problem definition.

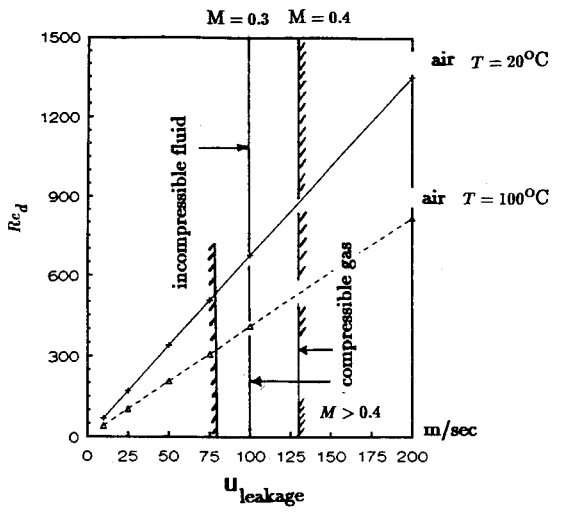

Fig. 2 Qualitatative diagram of the flow leakage vs Reynolds number.

physical properties of the air, pitch-to-diameter ratio of the brush, and the Reynolds number). This qualitative figure justifies an assumption of laminar and incompressible fluid since the Reynolds numbers are not in the turbulent range and the Mach number is less than 0.4. The authors have established through their experimental work[4,15,16] that the major factor contributing to the pressure drop is the longitudinal flow in the X direction in the XOY plane (Fig. 1). In order to simplify the model we assumed a two-dimensional flow and neglected both curvature effects and the flow in the Z direction (Fig. 1a). Data extracted from field experiments[10] showed time stable flow rates through the seal. Thus, the potential movements of the bristles do not have considerable influence on the level of the pressure drop and we adopted the assumption

of stationary bristles. While the flow inside the brush seal is laminar, flow in the seal cavity or the brush entry region can be turbulent and inherently unstable (see Sec. VI.C). Since our main interest will be concentrated on the brush core flow, we disregarded effects related to the potential inflow turbulence due to its limited impact on the overall pressure drop.

IV. Governing Equations

The computational domain (with L_x as length and L_y as width) is represented by the transversal brush cross section restricted by upper and lower walls (Fig. 1b). Inside the domain, the solid nonmoving bodies (bristles) of round cross section create a structure of n rows with m elements in each row. The bristle diameter is used as a characteristic length scale L_0 and the flow velocity at the entrance as a characteristic velocity U_0.

It is assumed that the flow is viscous and laminar and is caused by the pressure difference across the brush. The initial velocity distribution $u(x, y)$ and the characteristic pressure at the brush entrance are prescribed. The influence of the body forces is neglected and the flow is considered isothermal. The two-dimensional Navier–Stokes equations for unsteady incompressible viscous flow can be written in dimensionless conservative form as

$$\frac{\partial u}{\partial t} + \frac{\partial (uu)}{\partial x} + \frac{\partial (uv)}{\partial y} = -\frac{\partial P}{\partial X} + \frac{1}{Re}\left(\frac{\partial^2 u}{\partial x^2} + \frac{\partial^2 u}{\partial y^2}\right) \tag{1}$$

$$\frac{\partial v}{\partial t} + \frac{\partial (vv)}{\partial y} + \frac{\partial (uv)}{\partial x} = -\frac{\partial P}{\partial Y} + \frac{1}{Re}\left(\frac{\partial^2 v}{\partial x^2} + \frac{\partial^2 v}{\partial y^2}\right) \tag{2}$$

$$\frac{\partial u}{\partial x} + \frac{\partial v}{\partial y} = \mathcal{D} = 0 \tag{3}$$

Following the fundamentals of the marker-and-cell (MAC) concept,[22,23] a Poisson equation for pressure is obtained by the differentiation of Eqs. (1) and (2) and subsequent summation of the resulting equations:

$$\nabla^2 P = -\frac{\partial^2 (u^2)}{\partial x^2} - 2\frac{\partial^2 (uv)}{\partial x \partial y} - \frac{\partial^2 (v^2)}{\partial y^2} - \frac{\partial \mathcal{D}}{\partial t} + \frac{1}{Re}\left(\frac{\partial^2 \mathcal{D}}{\partial x^2} + \frac{\partial^2 \mathcal{D}}{\partial y^2}\right) \tag{4}$$

The procedure for determining pressures is based upon the requirement that the dilation term $\mathcal{D}$ vanishes[22,23] for every cell at the end of the time cycle ($\mathcal{D}^{n+1} = 0$). The solution of Eq. (4) requires an iterative process. After the pressure solution is converged (for a given velocity field), one can proceed with the next time step or iteration for the momentum equations. The remarkable aspect of Eq. (4) is that Eq. (3) just states that $\mathcal{D}$ is equal to zero. Because of incompatible initial conditions, or because of incomplete iterative solution of the Poisson equation, the finite difference approximation of $\mathcal{D}$ may not be equal to zero. The dilation term enforces satisfaction of continuity on the $n + 1$ time layer by imposing $\mathcal{D}^{n+1} = 0$. Welch et al.[22] showed that the continuity can be satisfied from the calculation of the new velocities, provided that Eq. (4) is accurately solved.

In this work, we are proposing a new technique for the flow solution in the brush. This involves brush partitioning and is intended to be a more suitable tool for large brush design and analysis. The technique allows the division of the brush in three typical areas (Fig. 1): 1) upstream free incoming flow zone and the first several rows of pins with developing flow, 2) a central core that consists of several rows of bristles with symmetric fully developed flow distribution, and 3) an outflow zone that includes the last rows of bristles and the downstream area where jet mixing and vortices generation are taking place. Hendricks[24] showed that the first three and last three rows of bristles are usually deflected outward of the brush core during the experiments and do not significantly contribute to the overall pressure drop. Since the central core has the highest level of packing density and flow resistance we will concentrate our analysis on this region. In general, the total pressure drop in cylinder arrays can be expressed as

$$\Delta P = C_z \sum \Delta P_{\text{av}}, \qquad i = 1, \ldots, N_{\text{rows}} \tag{5}$$

According to Zukauskas et al.,[17] $C_z = 1$, if the number of rows is greater than three. One can conclude that in terms of the pressure field, the flow is fully developed after passing through the first three rows. The assumption of a fully developed flow distribution in the central brush core reduces the size of the computational domain to a characteristic cell of several sequential rows (characterized by a constant ΔP_{av}), if indeed, one supplies proper symmetric, conservative boundary conditions.

A. Brush Entrance Region

We assume an entrance velocity profile with $u = f(y, t)$ and $v = f(y, t)$, which in most cases can be reduced to $u(x = 0) = 1$ and $v(x = 0) = 0$. In the case of lateral solid walls, the boundary conditions are specified as nonporous and nonslip, i.e., $u = v = 0$. In addition, for flow symmetry, the boundary conditions at the top and bottom boundaries are given as

$$\frac{\partial u}{\partial y} = 0 \quad \text{and} \quad \frac{\partial v}{\partial y} = 0 \tag{6}$$

or

$$\frac{\partial u}{\partial y} = 0 \quad \text{and} \quad v = 0 \tag{7}$$

Exit boundary conditions can be specified in a similar way:

$$\frac{\partial u}{\partial x} = 0 \quad \text{and} \quad v = 0 \tag{8}$$

B. Brush Core Zone

Inflow velocity conditions for this zone are the outflow conditions for the brush entrance zone

$$v = 0 \quad \text{and} \quad u = f_1(y, t) \tag{9}$$

where $f_1(y, t)$ is established from the solution of the Navier–Stokes equations in the entrance region. At the outflow of the computational domain we apply Eq. (8), and at the lateral walls Eqs. (6) and (7).

C. Brush Outflow Zone

Inflow velocity conditions for this area are calculated by means of the Navier–Stokes equations at the exit of the last repetitive brush core zone, which implies that $v = 0$ and $u = f_2(y, t)$. At the lateral walls we employ Eqs. (6) and (7) and the exit flow is allowed to develop naturally based on boundary conditions far downstream. Thus, the velocity boundary conditions imposed at the exit are derived from the satisfaction of the continuity equation (specifically in the direction of the U velocity)

$$\frac{\partial u}{\partial x} = -\frac{\partial v}{\partial y} \tag{10a}$$

and the condition for a fully developed velocity gradient for the vertical component

$$\frac{\partial v}{\partial x} = 0 \tag{10b}$$

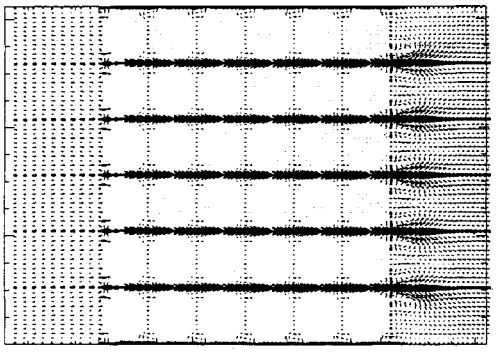

Fig. 3 Velocity–pressure decoupling (velocity and pressure are specified simultaneously at the inflow boundary).

D. Boundary Conditions for the Poisson Equation

The dynamic pressure P is determined from the balance of the normal forces with the inertia and viscous forces:

$$\frac{\partial P}{\partial x} = -\left[\frac{\partial(uu)}{\partial x} + \frac{\partial(uv)}{\partial y}\right] + \frac{1}{Re}\left(\frac{\partial^2 u}{\partial x^2} + \frac{\partial^2 u}{\partial y^2}\right) \quad (11)$$

$$\frac{\partial P}{\partial y} = -\left[\frac{\partial(uv)}{\partial x} + \frac{\partial(vv)}{\partial y}\right] + \frac{1}{Re}\left(\frac{\partial^2 v}{\partial x^2} + \frac{\partial^2 v}{\partial y^2}\right) \quad (12)$$

In combination with the Dirichlet conditions for the velocity, Eqs. (11) and (12) form a well-posed boundary-value problem with resulting solutions free of odd–even velocity–pressure decoupling,[25] as exemplified in Fig. 3.

E. Initial Conditions ($t = 0$)

The input velocities are given as $u = 1$ and $v = 0$. The pressures are set initially to an arbitrarily chosen value $P = P_{\text{ref}} = \text{const}$.

V. Numerical Implementation and Solution Procedure

The system of governing equations is discretized on a nonstaggered grid using the alternating direction method. The procedure uses the full direct approximation of each term within the differential equation on every half time step $\Delta\tau/2$. On each time step the u-v velocities and the pressure equation are solved jointly. The pressure equation solution uses a false-transient method. At each pressure iteration the reference point $P(1, 2)$ is assigned a value P^*. The pressure at every node is calculated from $\Delta P_{i,j} = P^* - P_{i,j}$. If the steady-state solution is of interest, then the internal pressure iterations are limited to one iteration $n_{\text{it}} = 1$ (two sweeps, one in the horizontal and one in the vertical direction). The computations are advancing in pseudotime until convergence is obtained. When using the fully implicit finite difference approximation the stability criteria for the solution of the pressure equation can be written as[22]

$$\Delta\tau_f \leq 1/(2)[\Delta x^2 \Delta y^2/(\Delta x^2 + \Delta y^2)] \quad (13)$$

The spatial derivatives, with the exception of the convection terms and cross derivatives, are approximated by an implicit second-order central finite difference. For the convective terms the implicit form of the first-order conservative upwind scheme proposed by Torrance[23] is employed. Other alternatives to the first-order upwinding, i.e., third-order-deferred correction scheme proposed by Kudriavtsev[26] and Hayase et al.[27] were also considered and implemented.[4] The details of the grid generation, the finite difference approximations, and the solution procedure are presented in Refs. 4, 18, 19, and 28. Issues of the iterative convergence and accuracy considerations were presented by these authors[4] to validate their numerical approach. The results demonstrated a very good coincidence of our numerical simulation with the experimental flow visualization of Bouard and Coutanceau.[4] The nondimensional pressure drops between the front and rear stagnation points[21] were also very close to the experimental and numerical data published by Fornberg.[29] A comparison of the experimental pressure drop obtained for three rows of packed cylinders in the staggered arrangement ($Re = 195$), and results of our numerical simulation obtained on 551 × 1281 mesh showed only a 7% difference.[21,28] Numerical grid convergence studies (grids 139 × 139, 278 × 278, 323 × 323, 415 × 415, and 645 × 645), performed for the flow in a staggered cylinder array,[20] showed grid independence both for the flow structures behind the cylinder and the global flow patterns.

VI. Results and Discussion

A. Pressure and Flow Patterns for Different Generic Brush Formations

The time-dependent flow and pressure developments in arrays of cylinders with $PTDR$ equal and smaller than unity were studied systematically.[18–20] The database that emerged showed that the development of flow and pressures around one cylinder, small groups of cylinders, and large groups of cylinders do not lend themselves to extrapolation from one configuration to another. A supporting example can be seen in the pressures of Figs. 4 and 5. Figure 4 presents the pressure oscillations at the trailing edge of a single cylinder located in the square channel of Fig. 1. It can be seen that in a quasi-steady regime the pressures in the wake of the cylinder reach a repetitive oscillatory profile within an envelope of ±5%. When the number of cylinders is increased to five (see also Fig. 8b) the pressure oscillations are contained within a ±10% envelope (Fig. 5a). The increase of the cluster to 72 cylinders (Fig. 6), arranged in a staggered formation of seven rows, generates in the wake of the array oscillatory pressures that can be contained within a ±2.5% envelope (Fig. 5b). These results, when considered in conjunction with the flow patterns already discussed,[18–20] demonstrate that phenomena indigenous to small arrays do not, as a rule, apply to large formations. Special methodologies, that involve the realistic treatment of boundary conditions, have to be applied to small arrays that can then be assembled in large clusters and render a realistic reproduction of the flow conditions.

Figure 6 presents the flow structure in an array of 7 × 11 round pins with $PTDR_L = PTDR_T = 1$. Along the walls, one can clearly observe high-velocity rivering jets that engender contiguous regions of lower pressure that attract the flow from the center of this generic brush.[20] The central region appears to be, fortunately, quite repetitive in nature, and indicates that the use of a repetitive cell for the construction of a large brush core is a feasible alternative. Finally, the wake region presents the formation of the exit jets and the incipient formation of meandering vortices.

The algorithm used to obtain the results presented in Fig. 6 ($PTDR = 1$) was used for modeling the dense array of Fig. 7. The flow, at $Re = 1000$, presents a steady-state pattern. This packing density ($PTDR_L = PTDR_T = 0.05$) is of significance for the real industrial brush seal applications ($1/10 \geq PTDR \geq 1/30$). The flow is dominated by accelerating–decelerating streams formed by the system of converging–diverging nozzles constituted by the adjacent cylinders. These flows that are characterized by extremely high convective gradients at their smallest cross section impose limitations on the algorithm in terms of computational stability, resolution, and global accuracy. Again, we see a repetitive symmetric flow structure in the core portion of the brush segment and flow symmetry around the channel centerline both inside and behind the array. The window marked in Fig. 7a is shown in detail in Fig. 7b. In Fig. 7b the rivering, lateral rivering, and

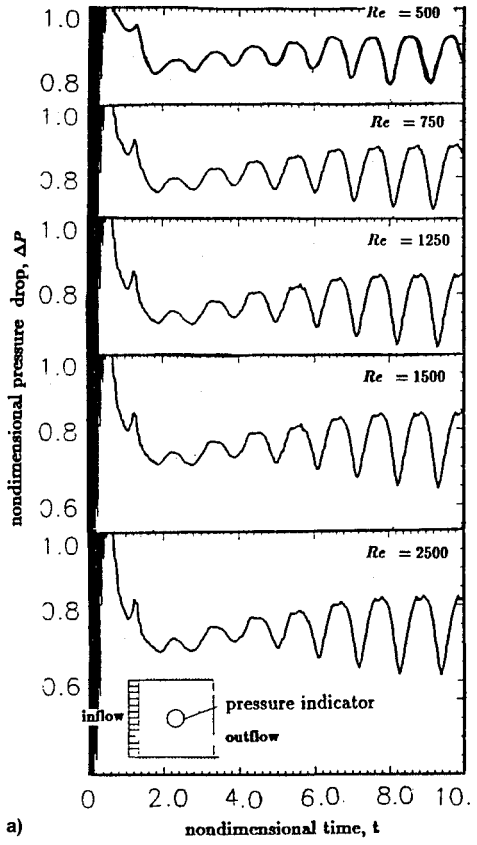

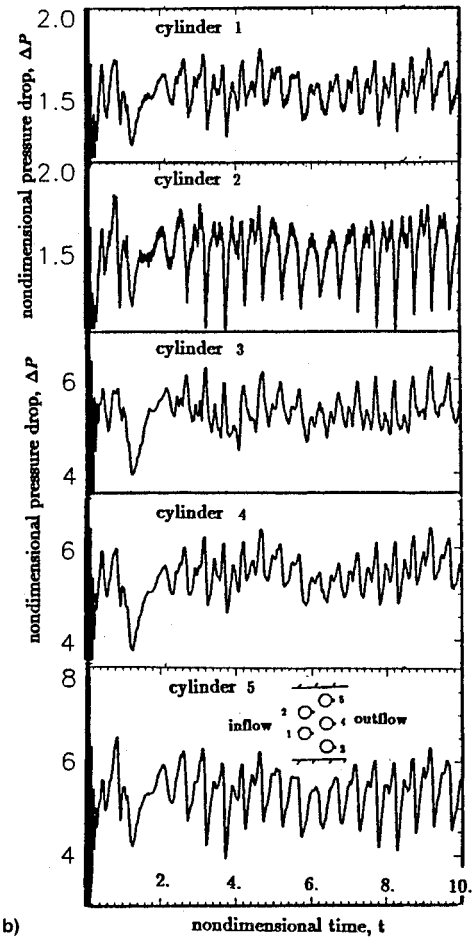

Fig. 4 Pressure development behind single cylinder (level 1) and small cluster of cylinders (level 2): a) single cylinder and b) small cluster in the square channel.

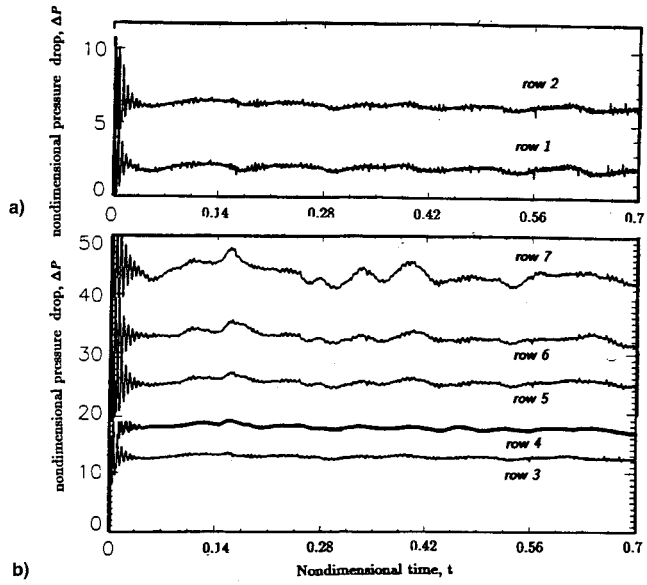

Fig. 5 Pressure development behind a large cluster of cylinders (level 3). Locations of the "pressure indicators" are shown in Fig. 6.

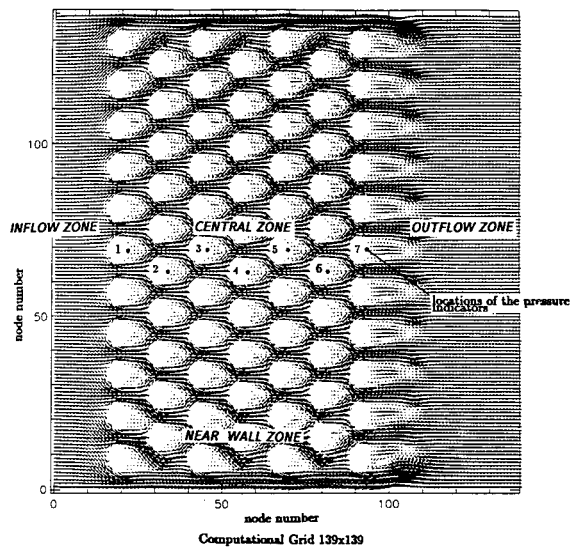

Fig. 6 Typical flow structure in a large cluster of cylinders (level 3).

the nozzle-jets are quite evident. The formation of the jets at the exit of the array can also be observed. The corresponding experimental results obtained by FFFT,[15,16] are shown in Fig. 7c. One can see good qualitative agreement between the experimental and numerical flowfields. In Fig. 8a one can see experimental results for a large pin array outflow that shows the interaction of 12 convective jets, both between themselves and with the walls. The experiment was run at $Re = 1000$, and a rather unusual "butterfly" flow formation was observed in the wake of the array. The high-speed, low-pressure region that developed near the walls of the pin array causes constant jet flow deviation towards the walls. The central void thus created is associated with pressures that are lower than the far downstream pressure. This pressure field configuration engenders a recirculation bubble that occupies a considerable part of the outflow cross section and consists of two butterfly-like vortices with strong negative flow along the centerline of the cross section. Exactly the same butterfly flow formation was obtained numerically for large and dense pin arrays (Fig. 7). Figures 8b and 8c present a simulation of this type of flow. Qualitatively, they present the same flow structure as in Fig. 8a, for the same Re number (1×10^3), even though the array

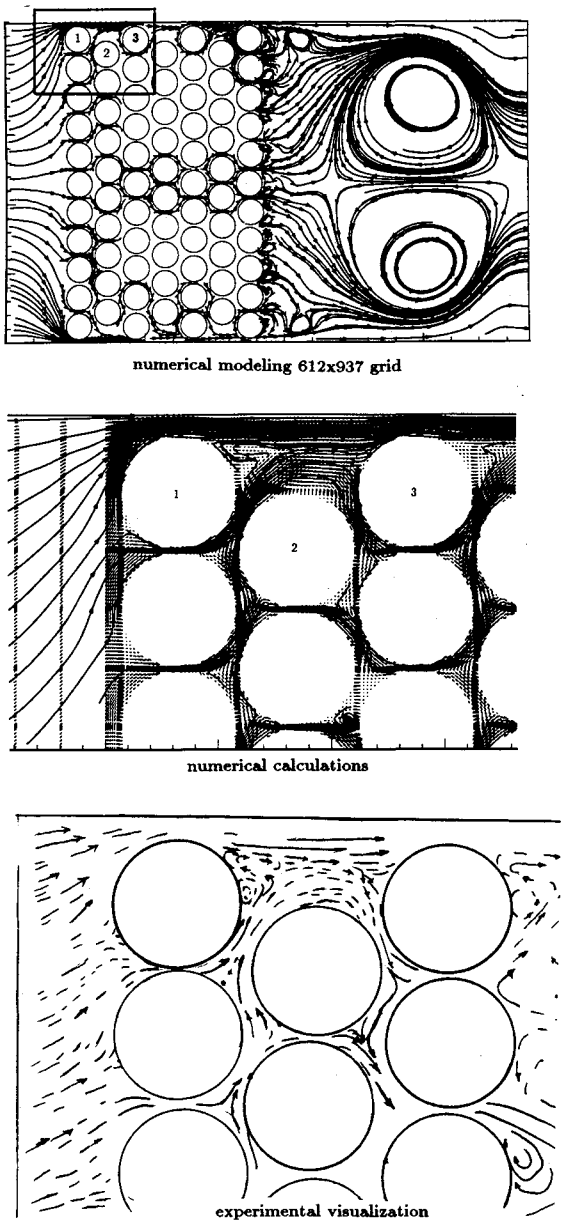

Fig. 7 Large cluster of densely packed cylinders at $Re = 195$ (level 4): a) flow through the cylinder's array and b) detail of flow near the wall marked at Fig. 7a. Comparison of numerical and experimental results.

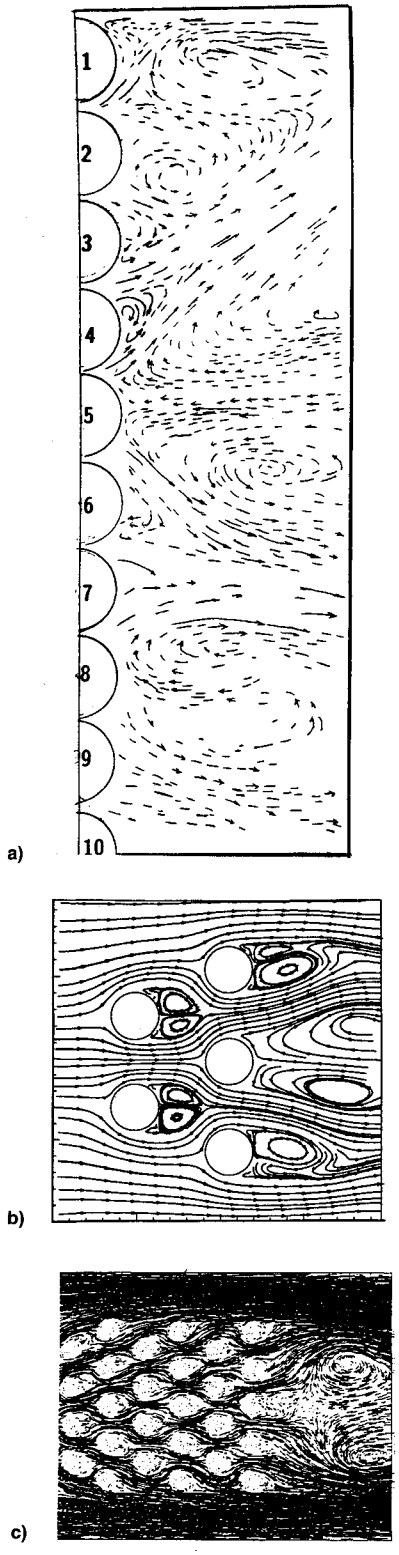

Fig. 8 Butterfly formation in the wake of the cylinder's clusters: a) experimental $Re = 1000$ (large array), b) numerical (small size array), and c) numerical (intermediate size array).

sizes are different and $PTDR = 1$. For the numerical results of Figs. 7, 8b, and 8c, it has been found that the flow structure inside the array converged to a steady solution much faster than the flow in the wake of the array. For $PTDR < 0.1$ the numerical solution can be obtained only by large-scale computational fluid dynamics modeling that requires grid sizes approaching 1000×1000 nodes. Any further increase in the size of the array or any further grid refinement becomes computationally prohibitive and appropriate strategies need to be found to handle this situation.

B. New Approach of Brush Segmentation and Assembly

The totality of the numerical and experimental work previously presented has led us to the conclusion[18] that we were rapidly approaching the limits of our computer modeling capacity. We have learned[18,28] the following:

1) The flow inside the brush reaches a convergent solution much sooner than near the wall boundaries or in the brush wake.

2) In deep clusters the flow is practically repetitive, as long as it is at least two rows away from the inlet or exit of the generic brush.

3) The pressures fall monotonically in the brush core portion.[4]

4) The computational time for calculating flow in a dense array of cylinders (3 rows $\times$ 11 lines) at moderate Re is prohibitive.

The numerical simulations shown in Fig. 9 explain the rationale of the brush partitioning approach. As mentioned earlier, one has to try to reduce the computational domain to a representative cell. To optimally define this cell, and its environment, several geometrical setups were chosen. The first considers the flow in the channel with no-slip walls as boundary conditions. The second replaces the wall with symmetry conditions at the boundary. From Figs. 9a and 9b one can see that the wall introduces near-wall effects that change considerably the flow structure. Thus, one has to select the symmetry boundary conditions as the optimal setup [see Eqs. (7), (8), and (10)]. At $Re = 100$ in the advanced time stages of the flow development one observes the incipience of an asymmetric mode in the outflow zone. This situation induces asymmetry in the central part of the brush segment (Figs. 9b and 9d). In larger (deeper) cylinder bundles this effect does not penetrate to their core (like in Fig. 6). Thus, the core and the outflow segments need to be treated as separate computational domains.

To respond to the modeling difficulties mentioned earlier, we assembled a full brush out of the component segments (inflow, core, and outflow). The continuity and momentum governing equations remain the same, but the boundary conditions were modified to take into the account the repetitive nature of the brush core. These boundary conditions were described by Eqs. (6–10). For the verification of the concept

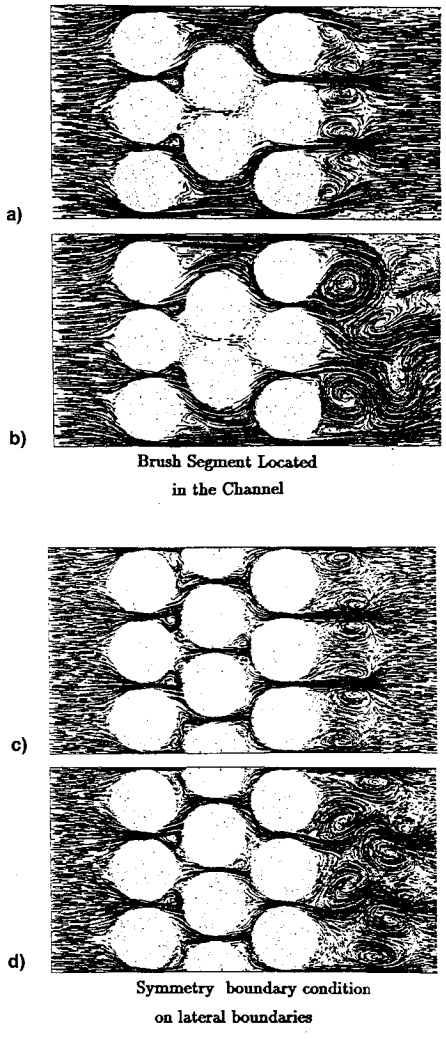

Fig. 9 Samples of the fluid flow in the brush segments at $Re = 100$: a) symmetric mode (initial stage of flow development), b) asymmetric mode (final stage of flow development), c) symmetric mode (initial stage of flow development), and d) asymmetric mode (final stage of flow development).

we have used a partitioned array that contains the segments shown in Fig. 9. Figure 10a presents a succession of identical core segments that are characterized by equal pressure drops. Figure 10b displays the inflow and outflow segments that are added to the central core in order to form a complete system. The resulting total pressure drop can be calculated as

$$\Delta P_{\text{brush}} = \Delta P_{\text{inflow}} + N^{\text{seg}}\Delta P_{\text{central}} + \Delta P_{\text{outflow}} \quad (14a)$$

If one considers the Hendricks[24] report, and if the brush has more than 10 rows ($N_{\text{rows}} \geq 10$), it seems rational that the overall pressure drop can be evaluated with little error by considering only what we defined as the core portion. Thus, one can simplify Eq. (19) to

$$\Delta P_{\text{brush}} = N^{\text{seg}}\Delta P_{\text{central}} \quad (14b)$$

C. Brush Seal Located in the Disk Interstage Cavity

The method presented in the previous sections is very efficient, but limits brush seal modeling to two-dimensional flows. Effects of the radial clearance between the brush and shaft, relative sizes of the backing and front plates, are not taken into consideration. The brush seal is usually designed with a brush preload of about 0.005 in., but many researchers reported experimental results with the brush/shaft clearances in the range between 0.0–0.0075 in. As reported by Yoder et al.,[30] seal leakage can significantly change as a function of the size of the clearance. To address these issues present authors have generated an integrated computational algorithm (FLOCON) to model complex interstage gas turbine cavity flow with the full brush seal inserted between adjacent cavities.[31] This algorithm builds up on the developments published previously[4,18] to predict brush permeability in the framework of the porous media model. The combination of the brush seal model (porous media assumption) and the interstage cavity (rotational axisymmetric flow) model was successfully implemented into a single computational entity. For example, Fig. 11 presents numerical flow visualization results of the two-dimensional axisymmetric rotational fluid flow ($Re = 10^5$) in a generic cross section of an interstage turbine cavity. The core flow is driven by an imposed pressure drop along the vane row of the main flow path. Three interconnected disk cavities separated by a brush seal are located along the secondary flow path. One of the important conclusions of these authors[31] is that for high main flow Reynolds numbers (always the case in the gas turbine flow path), the flow for-

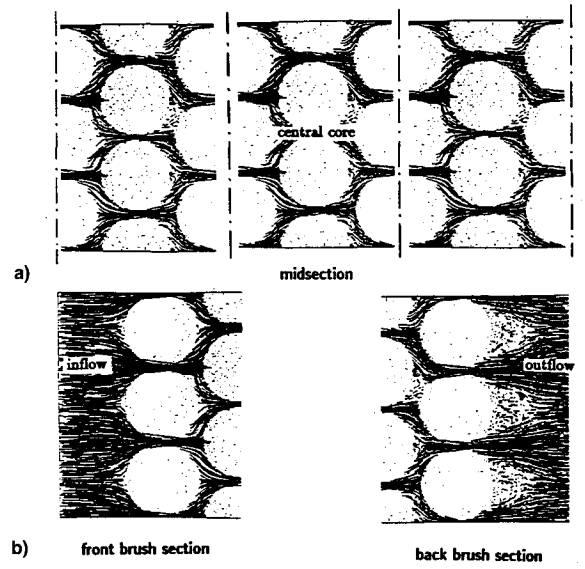

Fig. 10 Assembled brush cluster at $Re = 20$.

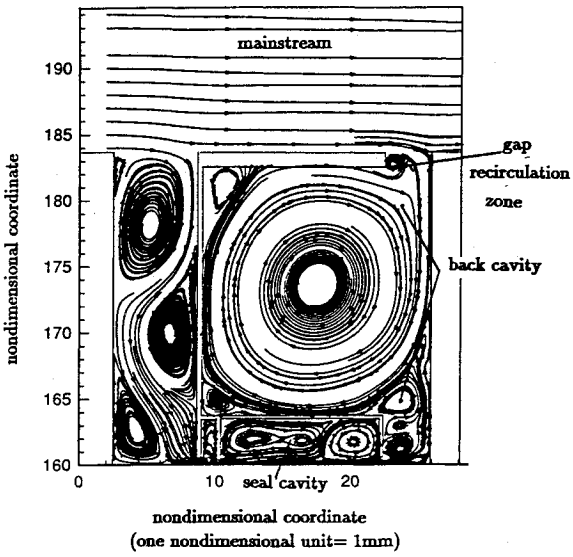

Fig. 11 Flow structure in the turbine interstage with the brush seal inserted in between two adjacent cavities ($Re = 10^5$).

mations in the seal cavity are extremely complicated and the fluid flow has a periodic oscillatory nature that requires time-dependent terms in the governing equations.

VII. Conclusions

The authors have presented chronologically the main stages and the main contributors to the technological development and numerical simulation of brush seals. As one can see, there were three avenues that were followed. The first involved laboratory experiments on simulated brush seals that led to a better understanding of the flow conditions and flow paths in the brush. The second involved industrial testing of brushes that yielded real experimental data concerning pressure drops and leakages. These efforts performed within the framework of major industrial manufacturers and users of brush seals led to the incorporation of brushes developed experimentally in these manufacturers' jet engines. The third and final avenue was the numerical development of design and predictive tools for the brushes. These tools have used either lumped or distributed codes, as shown earlier in this article. This article presented a first attempt at extending the distributed model of Braun and Kudriavtsev[4] to a model where the brush is segmented in inlet, core, and exit component. This concept allows the construction of infinitely large brushes with diminished computational penalty. It was shown that this concept predicts correctly the flow in the repetitive segments of the core, as well as in the inlet and exit zones. A further advance was made in this modeling by introducing a porous medium assumption to model the entirety of the brush, as it is inserted in the turbine cavity.

Acknowledgments

The authors are indebted to NASA Lewis Research Center, Cleveland, Ohio, and George Bobula, Robert Bill, and Robert Hendricks for their continued support.

References

[1]Hendricks, R. C., Carlile, G. A., and Liang A. D., "Some Sealing Concepts, Part B: Brush Seal Systems," *Fourth International Symposium on Transport Phenomena and Dynamics of Rotating Machinery* (Honolulu, HI), Vol. A, ISROMAC-4, 1992, pp. 265–276.

[2]Withers, P. A., "High Pressure Compressor Delivery Brush Seal of the International Aero Engines (IAE) V2500-A1 Gas Turbine Engine," *Proceedings of Seals Flow Code Development–92*, NASA Lewis Research Center, Cleveland, OH, 1992, pp. 275–279 (NASA CP-10124).

[3]Shapiro, W., and Artiles, A., "Industrial Code Development," *Proceedings of Seals Flow Code Development–92*, NASA Lewis Research Center, Cleveland, OH, 1992, pp. 13–67 (NASA CP-10124).

[4]Braun, M. J., and Kudriavtsev, V. V., "A Numerical Simulation of a Brush Seal Section and Some Experimental Results," *Journal of Turbomachinery*, Vol. 117, Jan. 1995, pp. 191–202; also *International Gas Turbine and AeroEngine Congress*, Cincinnati, OH, 1993, pp. 1–12 (ASME Paper 93-GT398).

[5]Liang, A. (ed.), "Seals Flow Code Development," NASA Lewis Research Center, NASA CP-10070, Cleveland, OH, March 1991.

[6]Chupp, R. E., and Holle, G. F., "Generalizing Circular Brush Seal Leakage Through a Randomly Distributed Bristle Bed," American Society of Mechanical Engineers Paper 94-GT-71, June 1994.

[7]Hendricks, R. C., Shlumberger, S., Braun, M. J., Choy, F., and Mullen, R. L., "A Bulk Flow Model of a Brush Seal System," American Society of Mechanical Engineers Paper 91-GT-325, 1991.

[8]Flower, R. "Brush Seal Development Systems," AIAA Paper 90-2140, 1990.

[9]Holle, G., and Krishnan, M., "Gas Turbine Engine Brush Seals Applications," AIAA Paper 90-2142, 1990.

[10]Chupp, R. E., and Dowler, C. A., "Performance Characteristics of Brush Seals for Limited-Life Engines," *Journal of Engineering for Gas Turbines and Power*, Vol. 115, April 1993, pp. 390–396.

[11]Dowler, C., "Air Force Brush Seal Programs," *Proceedings of Seals Flow Code Development–92*, NASA Lewis Research Center, Cleveland, OH, 1992, pp. 149–156 (NASA CP-10124).

[12]Basu, P., "Gas Seal Code Development and Analysis," *Proceedings of Seals Flow Code Development–92*, NASA Lewis Research Center, Cleveland, OH, 1992, pp. 167–169.

[13]Childs, D., "Dynamic Coefficients for Multiple Brush Seals," *Proceedings of Seals Flow Code Development–92*, NASA Lewis Research Center, Cleveland, OH, 1992, pp. 211–213 (NASA CP-10124).

[14]Caroll, P. F., and Easter B. P., "Brush Seal Would Impede Flow of Hot Gas," Rockwell International, *NASA Technical Briefs*, Vol. 17, No. 12, 1993, p. 83.

[15]Canacci, V. A., Braun, M. J., and Hendricks, R. C., "Flow Visualization and Motion Analysis for a Series of Four Sequential Brush Seals," *Journal of Propulsion and Power*, Vol. 8, No. 3, 1992, pp. 697–702.

[16]Braun, M. J., Canacci, V. A., and Russell, L. M., "Full Field Flow Visualization and Computer-Aided Velocity Measurements in a Bank of Cylinders in a Wind Tunnel," *Experiments in Fluids*, Vol. 13, 1992, pp. 117–127.

[17]Zukauskas, A., "Heat Transfer from Tubes in Crossflow," *Advanced Heat Transfer*, Vol. 8, 1972, pp. 93–160.

[18]Kudriavtsev, V. V., "Numerical Studies of the Transient Flows Within the Brush Seal Elements of the Aerospace Turbomachinery," Ph.D. Dissertation, Moscow Aviation Inst., School of Engine Technology, Moscow, Oct. 1993 (in Russian).

[19]Kudriavtsev, V. V., and Braun, M. J., "A Reynolds Number Parametric Numerical Investigation of Flow Structures and Pressure Distributions in a System of Cylinder Arrays," *Separated Flows/FED*, edited by J. C. Dutton and L. P. Purtell, Vol. 149, 1993, pp. 83–95.

[20]Braun, M. J., and Kudriavtsev, V. V., "Fluid Flow Structures in Staggered Banks of Cylinders Located in a Channel," *Journal of Fluids Engineering*, Vol. 117, March 1995, pp. 1–9.

[21]Braun, M. J., and Kudriavtsev, V. V., "Experimental and Analytical Investigation of Brush Seals," *Proceedings of Seals Flow Code Development–92*, NASA Lewis Research Center, Cleveland, OH, 1992, pp. 181–195 (NASA CP-10124).

[22]Welch, E. J., Harlow, F. H., Shannon, J. P., and Daly, B. J., "The MAC Method: A Computing Technique for Solving Viscous, Incompressible, Transient Fluid Flow Problems Involving Free Surfaces," Los Alamos Scientific Lab., Technical Rept., LA-3425,UC-32, TID-4500, 1966, pp. 1–146.

[23]Roache, P. L., *Computational Fluid Mechanics*, Hermosa Publishers, Albuquerque, NM, 1985.

[24]Hendricks, R. C., "Integrity Testing of Brush Seal in a T-700 Engine," *Proceedings of Seals Flow Code Development–92*, 1992, pp. 117–138 (NASA CP-10124).

[25]Patankar, S. V., *Numerical Heat Transfer and Fluid Flow*, Hemisphere, New York, 1980.

[26]Kudriavtsev, V. V., "New Higher-Order Finite Difference Scheme for Hyperbolic Conservation Law: HYBRID Approach," *Proceedings of the Modeling and Simulation Conference*, edited by W. G. Vogt and M. H. Mickle, Vol. 23, Pt. 5, Univ. of Pittsburgh, Pittsburgh, PA, 1992, pp. 2655–2662.

[27]Hayase, T., Humphrey, J. A. C., and Grief, R., "A Consistently Formulated QUICK Scheme for Fast and Stable Convergence Using Finite-Volume Iterative Calculation Procedures," *Journal of Computational Physics*, Vol. 98, 1992, pp. 108–118.

[28]Braun, M. J., and Kudriavtsev, V. V., "Brush Seal Numerical Simulation: Concepts and Advances," *Proceedings of Seals Flow Code Development–93*, 1993, pp. 159–195 (NASA CP-10136).

[29]Fornberg, F., "A Numerical Study of Viscous Flow Past a Circular Cylinder," *Journal of Fluid Mechanics*, Vol. 98, Pt. 4, 1980, pp. 819–855.

[30]Carlile, J. A., Hendricks, R. C., and Yoder, D. A., "Brush Seal Leakage Performance with Gaseous Working Fluids at Static and Low Rotor Speed Conditions," *Journal of Engineering for Gas Turbines and Power*, Vol. 115, 1993, pp. 397–403.

[31]Kudriavtsev, V. V., and Braun, M. J., "Interstage Disk-Cavity/Brush Seal Numerical Flow Visualization Study," *International Gas Turbine and AeroEngine Congress* (Houston, TX), 1995, pp. 1–13 (ASME Paper 95-GT).